Entropy production as a tool for characterizing nonequilibrium phase transitions

C. E. Fernández Noa, Pedro E. Harunari, M. J. de Oliveira, and C. E. Fiore
Instituto de Física da Universidade de São Paulo, 05314-970 São Paulo, Brazil

(Received 21 November 2018; published 3 July 2019)

Nonequilibrium phase transitions can be typified in a similar way to equilibrium systems, for instance, by the use of the order parameter. However, this characterization hides the irreversible character of the dynamics as well as its influence on the phase transition properties. Entropy production has been revealed to be an important concept for filling this gap since it vanishes identically for equilibrium systems and is positive for the nonequilibrium case. Based on distinct and general arguments, the characterization of phase transitions in terms of the entropy production is presented. Analysis for discontinuous and continuous phase transitions has been undertaken by taking regular and complex topologies within the framework of mean-field theory (MFT) and beyond the MFT. A general description of entropy production portraits for Z_2 ("up-down") symmetry systems under the MFT is presented. Our main result is that a given phase transition, whether continuous or discontinuous has a specific entropy production hallmark. Our predictions are exemplified by an icon system, perhaps the simplest nonequilibrium model presenting an order-disorder phase transition and spontaneous symmetry breaking: the majority vote model. Our work paves the way to a systematic description and classification of nonequilibrium phase transitions through a key indicator of system irreversibility.

DOI: 10.1103/PhysRevE.100.012104

I. INTRODUCTION

Thermodynamics states that while certain quantities including the energy are ruled by a conservation law, the entropy is not conserved. In the general case of a system coupled with an environment, the time variation of entropy dS/dt has two contributions: the flux to the reservoir Φ and the entropy production rate Π [1,2], that is,

$$\frac{dS}{dt} = \Pi(t) - \Phi(t). \tag{1}$$

Since in the steady state the time variation of S vanishes, $dS/dt = 0$, $\Pi = \Phi$ and all entropy produced must be delivered to the environment.

The entropy production has been the subject of considerable interest in physics [3–7], population dynamics [8], biological systems [9], experimental verification [10], and others. A microscopic definition of entropy production, in the realm of systems described by a master equation, is given by the Schnakenberg expression [11]:

$$\Pi(t) = \frac{k_B}{2}\sum_{ij}\{W_{ji}P_i(t) - W_{ij}P_j(t)\}\ln\frac{W_{ji}P_i(t)}{W_{ij}P_j(t)}, \tag{2}$$

where W_{ji} is the transition rate from the state i to state j with associated probability $P_i(t)$ at the time t, and W_{ij} denotes the reverse transition rate. Equation (2) implies that $\Pi(t)$ is always nonnegative because $(x-y)\ln(x/y) \geqslant 0$, vanishing when the detailed balance $W_{ij}P_j - W_{ji}P_i = 0$ is fulfilled. Thus, it distinguishes equilibrium from nonequilibrium systems. Defining the nonequilibrium entropy by $S(t) = -k_B\sum_i P_i(t)\ln P_i(t)$, a microscopic relation for the flux $\Phi(t)$ is obtained:

$$\Phi(t) = k_B\sum_{ij} W_{ij}\ln\frac{W_{ij}}{W_{ji}}P_j(t). \tag{3}$$

Equation (3) constitutes an alternative (and advantageous) formula for evaluating the steady entropy production, since it corresponds to an average that can be evaluated from the transition rates and it will be the subject of analysis in the present paper.

Despite the recent advances of stochastic thermodynamics, a fundamental question is whether entropy production can be utilized as a reliable tool for typifying nonequilibrium phase transitions. Different studies have been undertaken in this direction [4,7,8,12–18]. Some of them [4,7,8,18] indicate that continuous phase transitions can be identified by a divergence of the first derivative of Π whose associated exponent plays an analogous role to the specific heat. Other features, such as stochastic thermodynamics of many-particle systems at phase transitions to a synchronized regime have also been investigated [14,16,17]. Despite such a progress, a theoretical description of the entropy production at phase transition regimes, mainly in the context of discontinuous phase transition, has not been satisfactorily established yet.

In this paper we present a characterization of phase transitions in terms of the entropy production. Our study embraces the analysis of continuous and discontinuous phase transitions within the framework of mean-field theory (MFT) and beyond MFT. It is based on general considerations about the probability distribution related to the phase coexistence. The description of continuous phase transition takes into account the extension of finite-size scaling ideas and hyperscaling relations to nonequilibrium systems. A general description of entropy production for Z_2 ("up-down") symmetry systems in the realm of MFT is presented. Our main result is that a given

phase transition, whether continuous or discontinuous has a specific entropy production signature. As an example of our theoretical prescriptions, we shall consider the majority vote (MV) model with inertia [19–23]. It constitutes an ideal laboratory, since it presents continuous and discontinuous phase transition in both regular [19,23] and complex structures [20–22] displaying quite distinct features and universality classes. Thus, the existence of different entropy production hallmarks at phase transition regimes can be conveniently compared with those obtained from order parameter analysis.

This paper is organized as follows: In Sec. II we derive a general mean-field description for Z_2 ("up-down") symmetry systems. Sec. III presents a description of entropy production at phase transition regimes beyond the MFT. In Sec. IV, we exemplify our theoretical findings in the inertial MV model and Conclusions are performed in Sec. V.

II. GENERAL MEAN-FIELD DESCRIPTION FOR Z_2 ("UP-DOWN") SYMMETRY SYSTEMS

We are dealing with phase transitions in systems with up-down symmetry. Heuristically, a continuous phase transition in such class of models is described by the general logistic order-parameter equation:

$$\frac{d}{dt}m = a(q - q_c)m - bm^3, \tag{4}$$

where q denotes the control parameter and a and b are positive constants. It has two steady solutions: $m^{(D)} = 0$ (disordered phase) and $m^{(S)} = \pm\sqrt{a(q - q_c)/b}$ (ordered phase), stable for low and large values of q, respectively. The phase transition follows the mean-field exponent $\beta_{mf} = 1/2$ and m vanishes as $m \sim e^{a(q-q_c)t}$ for $q < q_c$ when $m \ll 1$. Conversely, one requires the inclusion of an additional term $+cm^5$ for reporting discontinuous phase transitions, leading to the following expression [23]:

$$\frac{d}{dt}m = a(q_b - q)m - bm^3 + cm^5, \tag{5}$$

where $c > 0$ [23]. It exhibits three steady-state solutions m: $m^{(D)} = 0$, $m^{(S)}$ and $m^{(U)}$. At $q = q_f = (b^2/4ac) - q_b$, m jumps from $m_1 \equiv m^{(S)}(q_f)$ to $m^{(D)} = 0$. For $q > q_f$, m behaves as $m \sim e^{a(q_b-q)t}$ for $m_0 \ll 1$ irrespective the initial condition $m_0 > 0$. The frontier $q = q_b$ separates the exponential vanishing of $m \sim e^{a(q_b-q)t}$ ($q > q_b$) from the convergence to a well definite $m_2 \equiv m^{(S)}(q)$ ($q < q_b$) when $m_0 \ll 1$. For $q_b < q < q_f$ (hysteretic branch), m behaves as follows: $m(t \to \infty) \to m^{(D)}$ if $m_0 < m^{(U)}$, $m(t \to \infty) \to m^{(S)}$ if $m_0 > m^{(U)}$ and only for $m_0 = m^{(U)}$ one has $m(t \to \infty) \to m^{(U)}$. For this reason $m^{(U)}$ is an unstable solution.

Since the above phenomenological relations hide the irreversible character which we are interested, we derive a general expression for the entropy production taking into account a generic dynamics with up-down symmetry. Each site i of an arbitrary lattice topology is attached to a spin variable σ_i that assumes the values ± 1. The transition rate is given by the expression $w(\sigma_i) = \frac{1}{2}[1 - q\sigma_i g(X)]$, with q denoting the control parameter and $g(X)$ expressing the generic dependence on a local neighborhood of k spins. Only two assumptions regarding $g(X)$ are required. The first is that due to the Z_2 symmetry, it depends on the sign of the local spin neighborhood (odd function). Also, taking into account that $w(\sigma_i)$ is constrained between 0 and 1, the product $|qg(X)| \leqslant 1$ for all values of X. These assumptions allow us to rewrite $g(X)$ as $g(X) = |g(X)|S(X)$, where $S(X)$ denotes the sign function: $\mathrm{sign}(X) = 1(-1)$ and 0, according to $X > 0 (< 0)$ and $X = 0$, respectively, where $|g(X)|$ gets restricted between 0 and $|g(k)|$.

From the master equation, one finds that the time evolution of order parameter $m = \langle\sigma_i\rangle$ is given by

$$\frac{d}{dt}\langle\sigma_i\rangle = -2\langle\sigma_i w(\sigma_i)\rangle. \tag{6}$$

In the steady state, $m = q\langle|g(X)|S(X)\rangle$. For the evaluation of Π, one requires the calculation of $w_i(\sigma)\ln[w_i(\sigma)/w_i(\sigma^j)]$ given by

$$\frac{1}{2}[\sigma_i S(X) - q|g(X)|S^2(X)]\ln\frac{1 - q|g(X)|}{1 + q|g(X)|}. \tag{7}$$

The reverse transition rate $w_i(\sigma^j)$ was obtained by performing the transformation $\sigma_i \to -\sigma_i$ resulting in $w_i(\sigma^j) = \frac{1}{2}[1 + q\sigma_i g(X)]$. The one-site MFT consists of rewriting the joint probability $P(\sigma_i, ..., \sigma_k)$ as a product of one-site probabilities $P(\sigma_i)...P(\sigma_k)$, from which one derives closed relations for the correlations and then the relevant quantities can be obtained as function of the control parameters. Since the main marks of critical and discontinuous phase transitions are not expected to depend on the particularities of $g(X)$, it is reasonable, within the MFT, to replace the averages in terms of an effective $\bar{g}$ given by

$$m = q\langle|g(X)|S(X)\rangle \to q\bar{g}\langle S(X)\rangle, \tag{8}$$

$$\frac{1}{2}\left\langle\sigma_i S(X)\ln\frac{1 - q|g(X)|}{1 + q|g(X)|}\right\rangle \to \frac{1}{2}\ln\frac{1 - q\bar{g}}{1 + q\bar{g}}\langle\sigma_i S(X)\rangle, \tag{9}$$

and

$$\frac{1}{2}\left\langle|g(X)|S^2(X)\ln\frac{1 - q|g(X)|}{1 + q|g(X)|}\right\rangle \to \frac{\bar{g}}{2}\ln\frac{1 - q\bar{g}}{1 + q\bar{g}}\langle S^2(X)\rangle. \tag{10}$$

At this level of approximation the steady entropy production then reads

$$\Pi = \frac{1}{2}\ln\frac{1 - q\bar{g}}{1 + q\bar{g}}[m\langle S(X)\rangle - q\bar{g}\langle S^2(X)\rangle]. \tag{11}$$

Above averages are calculated by decomposing the mean sign function in two parts:

$$\langle S(X)\rangle = \langle S(X_+)\rangle - \langle S(X_-)\rangle, \tag{12}$$

and

$$\langle S^2(X)\rangle = \langle S(X_+)\rangle + \langle S(X_-)\rangle, \tag{13}$$

with each term being approximated by

$$\langle S(X_\pm)\rangle = \pm\sum_{n=\lceil k/2\rceil}^{k} C_n^k p_\pm^n p_\mp^{k-n}, \tag{14}$$

where $\lceil ...\rceil$ is the ceiling function and for $S(X_+)[S(X_-)]$ the term C_n^k takes into account the number of possibilities of a neighborhood with n spins in the $+1[-1]$ states with associated probabilities $p_\pm = (1 \pm m)/2$. Equations (12) and (13) become simpler in the regime of large connectivities. To see

this, we first note that each term of the binomial distribution approaches a Gaussian with mean $kp_\pm$ and variance $\sigma^2 = kp_+p_-$, so that

$$\sum_{n=\lceil k/2\rceil}^{k} C_n^k p_\pm^n p_\mp^{k-n} \to \frac{1}{\sigma\sqrt{2\pi}} \int_{k/2}^{k} e^{-\frac{(\ell-kp_\pm)^2}{2\sigma^2}} d\ell = \frac{1}{2}\sqrt{\pi}\left\{\mathrm{erf}\left[\frac{k(1-p_\pm)}{\sqrt{2}\sigma}\right] - \mathrm{erf}\left[\frac{k(1/2-p_\pm)}{\sqrt{2}\sigma}\right]\right\}, \quad (15)$$

where $\mathrm{erf(x)} = 2\int_0^x e^{-t^2} dt/\sqrt{\pi}$ denotes the error function. Since for large k, $\mathrm{erf}[k(1-p_\pm)/\sqrt{2}\sigma] \to 1$ ($\langle S^2(X)\rangle \to 1$), the expressions for m and Π read

$$m = q\bar{g}\left[\mathrm{erf}\left(\sqrt{\frac{k}{2}}m\right)\right], \quad (16)$$

and

$$\Pi = \frac{1}{2}\ln\frac{1-q\bar{g}}{1+q\bar{g}}\left[\frac{m^2}{q\bar{g}} - q\bar{g}\right], \quad (17)$$

respectively. At the vicinity of the critical point m behaves as $m \sim (q-q_c)^{1/2}$. So that one reaches the following expressions for the entropy production:

$$\Pi \sim \frac{1}{2}\ln\frac{1+q\bar{g}}{1-q\bar{g}}\left[\frac{q_c-q}{q\bar{g}} + q\bar{g}\right], \quad (18)$$

for $q < q_c$, and

$$\Pi = \frac{q\bar{g}}{2}\ln\frac{1+q\bar{g}}{1-q\bar{g}}, \quad (19)$$

for $q > q_c$. Hence, the entropy production is continuous at the critical point q_c, with $\Pi_c = \frac{q_c\bar{g}}{2}\ln\frac{1+q_c\bar{g}}{1-q_c\bar{g}}$. However, its first derivative $\Pi' \equiv d\Pi/dq$ is discontinuous, jumping from

$$\Pi' = \frac{q_c\bar{g}^2}{1-q_c^2\bar{g}^2} + \frac{1-q_c\bar{g}^2}{2q_c\bar{g}}\ln\frac{1-q_c\bar{g}}{1+q_c\bar{g}}, \quad (20)$$

when $q \to q_c^-$, to

$$\Pi' = \frac{q_c\bar{g}^2}{1-q_c^2\bar{g}^2} - \frac{\bar{g}}{2}\ln\frac{1-q_c\bar{g}}{1+q_c\bar{g}}, \quad (21)$$

when $q \to q_c^+$, whose discontinuity of $-\frac{1}{2q_c\bar{g}}\ln\frac{1-q_c\bar{g}}{1+q_c\bar{g}}$ is associated with the critical exponent $\alpha_{mf} = 0$. Remarkably, having the classical exponents β_{mf} and γ_{mf} (evaluated from the order-parameter variance [24]), we see that the hyperscaling relation $\alpha_{mf} + 2\beta_{mf} + \gamma_{mf} = 2$ is satisfied, reinforcing that the criticality is signed by the jump in the first derivative of Π, in close similarity to the specific heat discontinuity for equilibrium systems.

Above MFT entropy production also predicts correctly the signatures at discontinuous phase transitions. According to Eq. (5), m jumps from $m_1 \equiv m^{(S)}(q_f)$ to 0 at $q = q_f = (b^2/4ac) - q_b$ and thereby from Eq. (17) the entropy production will jump from

$$\frac{1}{2}\left(q_f\bar{g} - \frac{m_1^2}{q_f\bar{g}}\right)\ln\left[\frac{1+q_f\bar{g}}{1-q_f\bar{g}}\right] \quad (22)$$

to

$$\frac{q_f\bar{g}}{2}\ln\left[\frac{1+q_f\bar{g}}{1-q_f\bar{g}}\right]. \quad (23)$$

Conversely, m jumps from 0 to $m_2 \equiv m^{(S)}(q_b)$ at $q = q_b$, and hence Π will jump from

$$\frac{q_b\bar{g}}{2}\ln\left[\frac{1+q_b\bar{g}}{1-q_b\bar{g}}\right] \quad (24)$$

to

$$\frac{1}{2}\left(q_b\bar{g} - \frac{m_2^2}{q_b\bar{g}}\right)\ln\left[\frac{1+q_b\bar{g}}{1-q_b\bar{g}}\right]. \quad (25)$$

The bistable behavior in the entropy production not only discerns continuous and discontinuous phase transitions but also it properly locates the hysteretic loop. In the Sec. IV, we show explicit results by taking an example of system with Z_2 symmetry.

III. BEYOND THE MEAN-FIELD THEORY

The analysis will be splitted in three parts: discontinuous transitions in regular lattices, complex networks, and continuous phase transitions.

A. Discontinuous phase transitions

1. Regular lattices

Distinct works [21–23,25] have attested that discontinuous phase transitions yield stark differences in regular and complex networks. In the former case, it emerges through sudden changes of $|m|$, its variance $\chi = N[\langle m^2\rangle - |m|^2]$ and other quantities whose scaling behavior goes with the system volume N [see, e.g., Figs. 5(b)–5(d)] [22,23,25]. At the vicinity of an arbitrary discontinuous phase transition point q_0, in which the correlation length is finite, the probability distribution can be approximately written down as a sum of two independent Gaussians, from which one extracts a scaling behavior with the system volume [23,25–27]. More specifically, the probability distribution is given by $P_N(m) = P_N^{(o)}(m) + P_N^{(d)}(m)$, where $P_N^{(\alpha)}(m)$ is associated to the phase α (with order-parameter m_α):

$$P_N^{(\alpha)}(m) = \frac{\sqrt{N}}{\sqrt{2\pi}}\frac{\exp\{N[\Delta q m - (m-m_\alpha)^2/(2\chi_\alpha)]\}}{[F_o'(\Delta q;N) + F_d'(\Delta q;N)]}. \quad (26)$$

Parameters χ_α and $\Delta q \equiv q_N - q_0$ correspond to the distribution width and the "distance" to the coexistence point q_0, respectively. Although in principle the assumption of two independent Gaussians can not describe properly a "weak" discontinuous phase transition, in which an overlap between $P_N^{(o)}(m)$ and $P_N^{(d)}(m)$ is expected, its reliability has been verified in several examples of nonequilibrium phase transitions with distinct properties [25,26], even in some cases in which the overlap is observed.

Despite the steady entropy production displaying a nontrivial dependence on the system features and on generic correlations of type $\langle\sigma_i\rangle$, $\langle\sigma_i\sigma_{i+1}\rangle$, $\langle\sigma_i\sigma_{i+1}\sigma_{i+2}\rangle$ and so on, Eq. (3) depicts it as the ensemble average of a fluctuating quantity, enabling resorting to the central limit theorem ideas. The generality of order-parameter distribution for tackling the

phase coexistence [25] and Eq. (3) setting up Φ as an ensemble average suggests the extension of a similar relationship for the steady entropy production. More concretely, we assume that $P_N(\phi) = P_N^{(o)}(\phi) + P_N^{(d)}(\phi)$, where $P_N^{(\alpha)}(\phi)$ is given by

$$P_N^{(\alpha)}(\phi) = \frac{\sqrt{N}}{\sqrt{2\pi}} \frac{\exp\{N[\Delta q\phi - (\phi-\phi_\alpha)^2/(2\bar{\chi}_\alpha)]\}}{[F_o(\Delta q;N) + F_d(\Delta q;N)]},$$

where each Gaussian is centered at ϕ_α with $\bar{\chi}_\alpha$ being the width of the α–th peak. Given that $P_N(\phi)$ is normalized, each term $F_{o(d)}$ then reads $F_{o(d)}(\Delta q;N) = \sqrt{\bar{\chi}_{o(d)}}\exp\{N\Delta q[\phi_{o(d)} + \bar{\chi}_{o(d)}\Delta q/2]\}$. The steady entropy production $\Pi = \Phi$ is straightforwardly calculated from $P_N(\phi)$, $\Phi = \int_{-\infty}^{\infty}\phi P_N(\phi)d\phi$, reading

$$\Pi = \sum_{\sigma=o,d} \frac{(\phi_\sigma + \bar{\chi}_\sigma\Delta q)\,F_\sigma(\Delta q;N)}{F_o(\Delta q;N) + F_d(\Delta q;N)}. \tag{27}$$

Close to the phase coexistence, in which Δq is expected to be small, the terms $O(\Delta q)$ dominate over $O(\Delta q)^2$ and Eq. (27) can be approximately rewritten as

$$\Pi = \frac{\sqrt{\bar{\chi}_o}\phi_o + \sqrt{\bar{\chi}_d}\phi_d e^{-N[(\phi_o-\phi_d)\Delta q]}}{\sqrt{\bar{\chi}_o} + \sqrt{\bar{\chi}_d}e^{-N[(\phi_o-\phi_d)\Delta q]}}. \tag{28}$$

Note that the Eq. (28) reproduces the jump from $\phi_o(\phi_d)$ when $\Delta q \to 0_{-(+)}$ and $N \to \infty$ (a third reason for assuming $P_N(\phi)$ as a sum of independent Gaussians). Remarkably, the curves for different values of N cross at the transition point $\Delta q = 0$ with

$$\Pi^* = \frac{\sqrt{\bar{\chi}_o}\phi_o + \sqrt{\bar{\chi}_d}\phi_d}{\sqrt{\bar{\chi}_o} + \sqrt{\bar{\chi}_d}}. \tag{29}$$

The crossing point clearly discerns continuous and discontinuous phase transitions and can be used as an indicator of the phase coexistence, as shown in Figs. 5 and 8 and in Ref. [28] (Figs. 7 and 8) for a chemical reaction model.

2. Complex networks

Distinct works [21–23,29] have stated that in contrast to regular structures, the phase coexistence in complex networks is akin to the MFT (see, e.g., Fig. 1), whose behavior is generically characterized by the existence of a hysteretic loop and bistability. The order parameter will present a spinodal line in which along the hysteretic loop the system will converge to one of the possible steady states depending on the initial configuration. For locating the "forward transition" point q_f, the system is initially placed in an ordered configuration and the tuning parameter q is increased by an amount δ, whose final state at q is used as the initial condition at $q+\delta$ until the order-parameter discontinuity is viewed. Conversely, the "backward transition" point q_b is pinpointed by starting from the disordered phase and decreasing q (also by the increment δ) until the order-parameter jump takes place. Entropy production also captures these features, which can be viewed through a general argument for order-disorder phase transitions. The order-parameter behaves as $\langle\sigma_i\rangle \sim N^{-1/2}$ in the disordered phase and then a n–th correlation will behave as $\langle\sigma_i\sigma_{i+1}...\sigma_{i+n}\rangle \approx \langle\sigma_i\rangle\langle\sigma_{i+1}\rangle...\langle\sigma_{i+n}\rangle = N^{-n/2}$. Hence in the thermodynamic limit, all correlations will vanish in the disordered phase and Π will depend solely on control parameters.

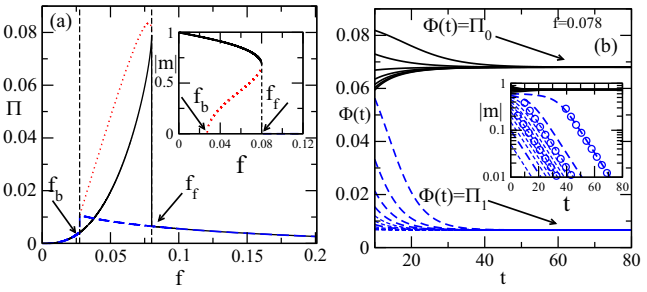

FIG. 1. Panel (a) depicts the bistable behavior of Π for $\theta = 0.43$ and $k = 12$. Continuous (dashed) curves denote the stable solutions for $m_0 > m^{(U)}$ ($m_0 < m^{(U)}$). They coincide for $f > f_f$ and $f < f_b$ and are different for $f_b < f < f_f$. Dotted curves correspond the unstable solutions for $f_b < f < f_f$ with $m = m^{(U)}(f)$ if $m_0 = m^{(U)}(f)$. Inset: The same but for the order-parameter. In panel (b) the time evolution of flux $\Phi(t)$ for distinct initial configurations and $f = 0.078$. Inset: The time evolution of m, where circles correspond to the function $m \sim e^{a(f_b-f)t}$, valid for $m_0 \ll 1$.

Contrariwise, $\langle\sigma_i\sigma_{i+1}...\sigma_{i+n}\rangle$ presents a well defined (nonzero) value in the ordered phase and Π depends not only on the control parameters but also on correlations. So that, the jumps at q_f (from $m_1 \equiv m(q_f) \neq 0$ to 0) and q_b (from 0 to $m_2 \equiv m(q_b) \neq 0$), commonly viewed in terms of order-parameter, will also be present in the entropy production. The presence of bistability implies that $\Phi(t)$ will converge to one of the two well defined values, since along the hysteretic branch the system behaves just like the disordered or the ordered phase, depending on the initial condition. Although the above argument is valid for a generic order-disorder phase transition, it is expected to describe phase transitions different from the order-disorder ones, provided the order-parameter and correlations also present a hysteretic behavior. Thereby, both cases reveal that the entropy production behavior also embraces phase coexistence traits commonly treated in terms of the order-parameter.

B. Continuous phase transitions

Albeit characterized by the vanishing of the order-parameter $|m|$ and algebraic divergences of other quantities at the criticality, the behavior of quantities become rounded due to finite size effects. According to the standard finite-size scaling (FSS), they behave as $|m| = N^{-\beta/\nu}\tilde{f}(N^{1/\nu}|\epsilon|)$, $\chi = N^{\gamma/\nu}\tilde{g}(N^{1/\nu}|\epsilon|)$ with $\tilde{f}$ and $\tilde{g}$ being scaling functions and $\epsilon = (q-q_c)/f_c$. Typically, q_c is located by choosing a quantity that intersects for distinct system sizes. For order-disorder phase transitions, the quantity U_4 fulfills the above requirement, whose crossing value U_0^* depends on the lattice topology and the symmetry properties. Some papers [4,5] have described similar scaling relation for the entropy production. Close to the criticality Π and its first derivative $\Pi' \equiv d\Pi/dq$ behave as $\Pi - \Pi_c \sim (q_c - q)^{1-\alpha}$ and $\Pi' \sim (q_c-q)^{-\alpha}$, respectively. Above expression states that Π is continuous, but the derivative Π' diverges at $q = q_c$. Due to finite-size effects, it is reasonable to assume that Π' behaves as $\Pi' = N^{\alpha/\nu}\tilde{h}(N^{1/\nu}|\epsilon|)$, with $\tilde{h}$ being an appropriate scaling function. From the exponents β, α and γ, we wish to check

whether the hyperscaling relation $\alpha + 2\beta + \gamma = 2$, fulfilled in the MFT approach, is also satisfied beyond the MFT. Here we extend the entropy production analysis for continuous phase transitions in random complex topologies.

IV. APPLICATIONS: THE INERTIAL MAJORITY VOTE (MV) MODEL

A. Model and definitions

The previous predictions will be exemplified in one of the simplest nonequilibrium phase transition model with steady states, the majority vote (MV) model [19,20], defined as follows: Each site i of an arbitrary lattice can assume $\bar{q}$ possible integer values ($\sigma_i = 0, 1, ..., \bar{q} - 1$). The dynamics is ruled by the fraction $\bar{w}_X$ of neighboring nodes in each one of the $\bar{q}$ states plus a local spin dependence $\theta\delta(\sigma_i', \sigma_i)$ (an inertial term), $\bar{w}_{\sigma_i'} = (1-\theta)\sum_{j=1}^{k}\delta(\sigma_i', \sigma_j)/k + \theta\delta(\sigma_i', \sigma_i)$, with σ_j denoting the spin of each one of the k nearest neighbors of the site i. With probability $1 - f$ (f being the misalignment parameter) the local spin σ_i changes to the majority neighborhood spin σ_i' and with complementary probability f the majority rule is not followed. For $\bar{q} = 2$ and $\theta = 0$, the MV becomes equivalent to the Ising model in contact with two heat reservoirs, one being a source of heat, at infinite temperature, and the other a sink of heat, at zero temperature [19]. The contact with the first occurs with a given probability and with the second with the complementary probability. Recent studies [21–23] revealed that large inertia shifts the phase transition to a discontinuous one for all values of $\bar{q}$. An order-disorder phase transition arises by increasing f, whose classification depends on θ and the lattice connectivity k. For low $\bar{q}$ ($\bar{q} < 4$) and $\theta = 0$ (inertialess regime), it is always continuous [19–21], but the increase of $\bar{q}$ modifies the symmetry properties (Z_2 and C_{3v} for $\bar{q} = 2$ and 3, respectively), leading to different sets of critical exponents. The phase transition becomes discontinuous for larger k's when θ goes up [21,23]. A given nth order parameter moment $\langle m^n\rangle$ is calculated through the quantity $\langle m^n\rangle = \langle|\sum_{i=1}^{N} e^{2\pi i\sigma_i/\bar{q}}/N|^n\rangle$, with $\langle ...\rangle$ denoting the ensemble average. The $n = 1$ is a reliable order-parameter since $m > 0$ ($= 0$) in the ordered (disordered) phases. The steady entropy production rate is calculated from Eq. (3) through the expression

$$\Pi = \frac{k_B}{N}\left\langle \sum_{j=1}^{\bar{q}-1}\sum_{i=1}^{N} w_i(\sigma)\ln\frac{w_i(\sigma)}{w_i(\sigma^j)}\right\rangle, \tag{30}$$

with $w_i(\sigma)$ and $w_i(\sigma^j)$ being the transition rate and its reverse, respectively. The latter is evaluated by taking transformation of σ_i to one of its $\bar{q} - 1$ distinct values. For $\bar{q} = 2$, the transition rate above is more conveniently rewritten by taking the transformation $\sigma_i \to 2\sigma_i - 1$, so that $w_i(\sigma)$ and m reads $w_i(\sigma) = \frac{1}{2}[1 - (1-2f)\sigma_i S(X)]$ and $m = \langle\sigma_i\rangle$, respectively, where $S(X)$ again denotes the sign function evaluated over the local neighborhood plus the inertia $X = (1-\theta)\sum_{j=1}^{k}\sigma_j/k + \theta\sigma_i$. Thus, in such case X not only depends on the neighborhood, but also on the local spin σ_i. The steady-state expression for the absolute m reads

$$m = (1-2f)\langle S(X)\rangle. \tag{31}$$

To evaluate Π from Eq. (30) we take the ratio between $w_i(\sigma)$ and its reverse $w_i(\sigma^j)$ given by

$$\frac{w_i(\sigma)}{w_i(\sigma^j)} = \frac{1-(1-2f)\sigma_i S\left[\sum_{j=1}^{k}\sigma_j + \frac{k\theta}{1-\theta}\sigma_i\right]}{1+(1-2f)\sigma_i S\left[\sum_{j=1}^{k}\sigma_j - \frac{k\theta}{1-\theta}\sigma_i\right]}. \tag{32}$$

Inspection of the ratio above reveals that only local configurations with $|\sum_{j=1}^{k}\sigma_j|$ greater than $k\theta/(1-\theta)$ will contribute for Π, since only in these cases the ratio is different from 1. Thereby, it can be rewritten as $w_i(\sigma)/w_i(\sigma^j) = \sigma_i S'(X)\ln[f/(1-f)]$, with $S'(X)$ being the sign function evaluated only over the subspace of local configurations in which the ratio is different from 1 (for $\theta = 0$, it reduces to the usual sign function). The expression for Π is then given by

$$\Pi = \frac{1}{2}\ln\frac{f}{1-f}[\langle\sigma_i S'(X)\rangle - (1-2f)\langle S'^2(X)\rangle], \tag{33}$$

in such a way that it depends on the averages $\langle\sigma_i S'(X)\rangle$ and $\langle S'^2(X)\rangle$.

B. MFT results

The (general) results from Sec. II can be straightforwardly applied for the inertialess regime simply by replacing q and $g(X)$ for $1 - 2f$ and $S(X)$, respectively. Although the main aspects of phase transitions are expected not depending on θ, in such case it is more convenient to use Eq. (33), due to the dependence on the local spin. The MFT expression for m reads

$$m = (1-2f)\left[\langle S[X_+]\rangle\left(\frac{1+m}{2}\right) - \langle S[X_-]\rangle\left(\frac{1-m}{2}\right)\right]. \tag{34}$$

As in Sec. II, for large k the $\langle S[X_\pm]\rangle$ can be calculated from Eq. (14), but the lower limits $n_\pm$ depend on θ and are given by

$$n_+ = \frac{k(1-2\theta)}{2(1-\theta)} \quad \text{and} \quad n_- = \frac{k}{2(1-\theta)}.$$

Note that both $n_\pm$ reduce to $k/2$ when $\theta = 0$. By performing similar calculations that those from Sec. II, Eq. (34) in the regime of large connectivities becomes

$$m = \frac{(1-2f)[\mathrm{erf(a)} - \mathrm{erf(b)}]}{2-(1-2f)[\mathrm{erf(a)} + \mathrm{erf(b)}]}, \tag{35}$$

where erf(x) denotes the error function, with a and b given by

$$a = \sqrt{\frac{k}{2}}\left[\frac{\theta}{1-\theta} + m\right] \quad \text{and} \quad b = \sqrt{\frac{k}{2}}\left[\frac{\theta}{1-\theta} - m\right]. \tag{36}$$

As performed previously, the one-site MFT for Π is obtained by replacing $\langle\sigma_i S'(X)\rangle$ for $\langle\sigma_i\rangle\langle S'(X)\rangle$, so that

$$\Pi = \frac{1}{2}\ln\frac{f}{1-f}[m\langle S'(X)\rangle - (1-2f)\langle S'^2(X)\rangle]. \tag{37}$$

Figure 1 summarizes the main results for the former case for $k = 12$ and distinct inertia values. As predicted in Sec. II, the order parameter jumps at f_f and f_b and the discontinuities are also presented in the entropy production. Along the hysteretic branch, $\Phi(t)$ converges to two well defined values

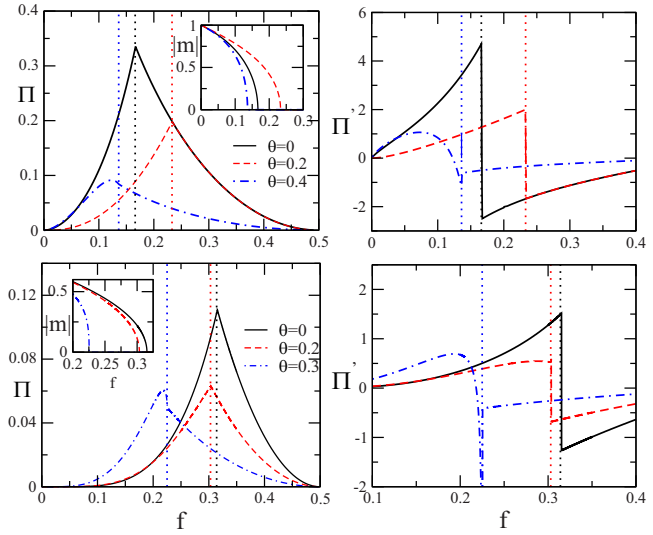

FIG. 2. Left and right panels: Steady entropy production Π and its derivative Π′ versus f for low θ, $k = 4$ (top) and $k = 12$ (bottom), respectively. Inset: the corresponding order parameter versus f. Dotted lines denote the associated critical points.

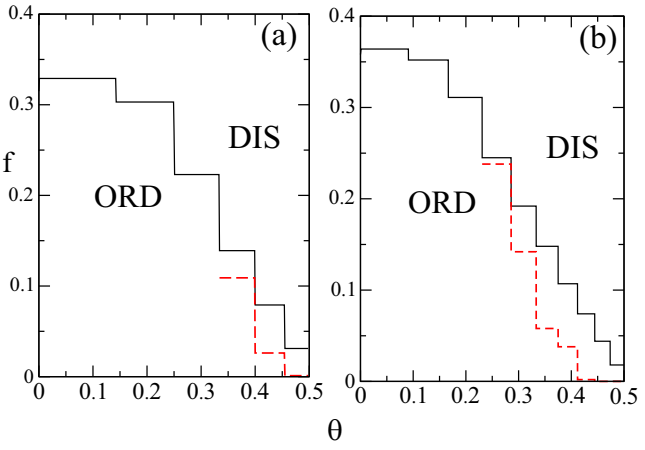

FIG. 3. Panels (a) and (b) show the mean-field phase diagrams for $k = 12$ and $k = 20$ through analysis of entropy production. ORD (DIS) denote the ordered (disordered) phases, whereas continuous and dashed lines, correspond to the values of f_f and f_b, respectively. They coincide for continuous transitions, but are different for discontinuous ones.

which are $\Pi_1 \equiv \Pi(f, \theta)$ and $\Pi_0 \equiv \Pi(m^{(S)}, f, \theta)$ in the region $f_b < f < f_f$. The time evolution of m follows theoretical prediction $m \sim e^{a(f_b - f)t}$ for $m_0 \ll 1$ (see inset symbols).

Figure 2 exemplifies the main results for continuous phase transitions. In all cases, the entropy production increases until a maximum at $f = f^*$ and then decreases for $f > f^*$. For the inertialess case or even the low θ, $f^* = f_c$. This can be understood by resorting the findings from Sec. II [for $q = 1 - 2f$ and $g(X) = S(X)$] in which in the regime of large k, m and Π are given by

$$m = (1 - 2f)\mathrm{erf}\left(m\sqrt{\frac{k}{2}}\right), \tag{38}$$

and

$$\Pi = \frac{1}{2}\ln\frac{f}{1-f}\left[\frac{m^2}{1-2f} - (1-2f)\right], \tag{39}$$

respectively. At the vicinity of the critical point, where m is expected to be small, the right side of Eq. (38) can be expanded in Taylor series, allowing us to rewrite m solely in terms of f and k:

$$m \sim \sqrt{\frac{12}{k}}(f_c - f)^{1/2}, \tag{40}$$

where $\beta_{mf} = 1/2$ is the critical exponent and

$$f_c = \frac{1}{2}\left\{1 - \sqrt{\frac{\pi}{2k}}\right\}, \tag{41}$$

is the critical point. From Eq. (40), Π behaves as $\Pi \approx \frac{1-2f}{2}\ln\frac{1-f}{f}[1 - \frac{12}{k}\frac{f_c - f}{(1-2f)^2}]$ and $\Pi = \frac{1-2f}{2}\ln\frac{1-f}{f}$ for $f \to f_c^-$ and $f > f_c$, respectively, and hence Π is continuous at the criticality. Despite this, its first derivative Π′ jumps from $\frac{1}{2}\sqrt{\frac{\pi}{2k}}\ln\frac{1+\sqrt{\frac{\pi}{2k}}}{1-\sqrt{\frac{\pi}{2k}}}$ to $\frac{12}{\pi}\ln\frac{1+\sqrt{\frac{\pi}{2k}}}{1-\sqrt{\frac{\pi}{2k}}}$, hence consistent with the exponent $\alpha_{mf} = 0$. By increasing θ (see, e.g., $\theta = 0.4$ and 0.3 for $k = 4$ and $k = 12$, respectively), the maximum of Π does not coincide with the jump of Π′ nor the order-parameter vanishing. Thereby the present results (together with the general description in Sec. II) unifies the description in the MFT context, in which the criticality is not necessarily marked by a peak in the entropy production but related to a peculiar behavior of its first derivative.

Last, in Fig. 3 we plot the phase diagrams for $k = 12$ and $k = 20$ evaluated through the distinct entropy production signatures. We see that both phase transition location and its classification are in full agreement with those obtained from order-parameter analysis (see, e.g., Fig. 1 in Ref. [21]).

A final comment concerns that the limit $k \to \infty$ corresponds to the complete graph regime. In this case, the expression for m and Π become

$$m = \frac{(1-2f)\left[S\left(\frac{\theta}{1-\theta} + m\right) - S\left(\frac{\theta}{1-\theta} - m\right)\right]}{2 - (1-2f)\left[S\left(\frac{\theta}{1-\theta} + m\right) + S\left(\frac{\theta}{1-\theta} - m\right)\right]}, \tag{42}$$

and

$$\Pi = \ln\frac{f}{1-f}\{m - (1-2f)Y_p\}, \tag{43}$$

respectively, where $Y_p = \{(1+m)S[m + \theta/(1-\theta)] - (1-m)S[m - \theta/(1-\theta)]\}/2$. By combining the above relation with Eq. (42), it follows that $\Pi = 0$ and thus there is no entropy production in the complete graph case. The reversible character of the inertialess MV in the complete graph has already been presented in Ref. [30] and our analysis not only confirms it but also extends for the inertial regime.

C. Beyond the MFT: Numerical results in regular and complex structures

Numerical simulations will be performed for distinct lattices structures and neighborhoods. All studied structures are quenched, i.e., they do not change during the simulation

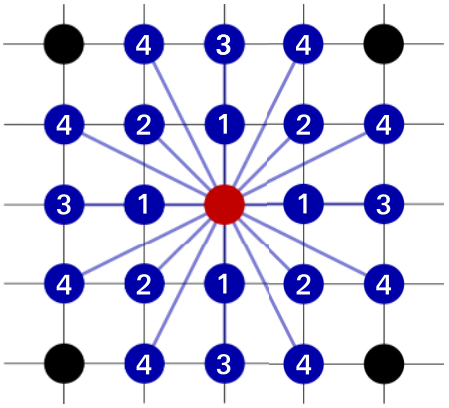

FIG. 4. Local configuration for a bidimensional lattice with central site (red) and its first (1), second (2), third (3), and fourth (4) next neighbors.

of the model. For a given network topology with N, f, and θ held fixed, a site i is randomly chosen, and its spin value σ_i is updated ($\sigma_i \to \sigma_i'$) according to $\bar{w}_{\sigma_i'} = (1-\theta)\sum_{j=1}^{k}\delta(\sigma_i', \sigma_j)/k + \theta\delta(\sigma_i', \sigma_i)$, with σ_j denoting the spin of each one of the k nearest neighbors of the site i. With probability $1-f$, σ_i changes to the majority neighborhood spin σ_i' and with complementary probability f the majority rule is not followed. A Monte Carlo (MC) step corresponds to N updating spin trials. After repeating the above dynamics a sufficient number of MC steps (in order of 10^6 MC steps), the system attains a nonequilibrium steady state.

Random regular networks have been generated through a configuration model scheme [31] described as follows: For a system with N nodes and connectivity k, we first start with a set of Nk points, distributed in N groups, in which each one contains exactly k points. Next, one chooses a random pairing of the points between groups and then creates a network linking the nodes i and j if there is a pair containing points in the ith and jth sets until $Nk/2$ pairs (links) are obtained. If the resulting network configuration present a loop or duplicate links, then the above process is restarted.

The increase of connectivity k in bidimensional topologies is accomplished by extending the range of interaction neighborhood. For example, $k = 4, 8, 12$, and 20 includes interaction between the first, first and second, first to third and first to fourth next neighbors, respectively, as sketched in Fig. 4.

1. Discontinuous phase transitions

Figure 5 exemplifies such predictions for the MV in bidimensional lattices with $k = 20$ and $\theta = 0.375$. The entropy production curves follow the theoretical predictions [continuous lines in Figs. 5(a) and 5(b)] from Eqs. (28) and (29), whose intersection among curves [Figs. 5(a) and 5(b)] occurs at $f_0 = 0.05084(5)$, in excellent agreement with estimates obtained from standard techniques [25], 0.0509(1) (maximum of χ), 0.0510(1) (minimum of $U_4 = 1 - \langle m^4\rangle/3\langle m^2\rangle^2$), and 0.0509(1) [equal area order-parameter distribution $P_N(m)$]; see, e.g., Fig. 5(d). Collapse of all data by taking the transformation $y = (f - f_0)N$ (inset) reinforces the reliability of

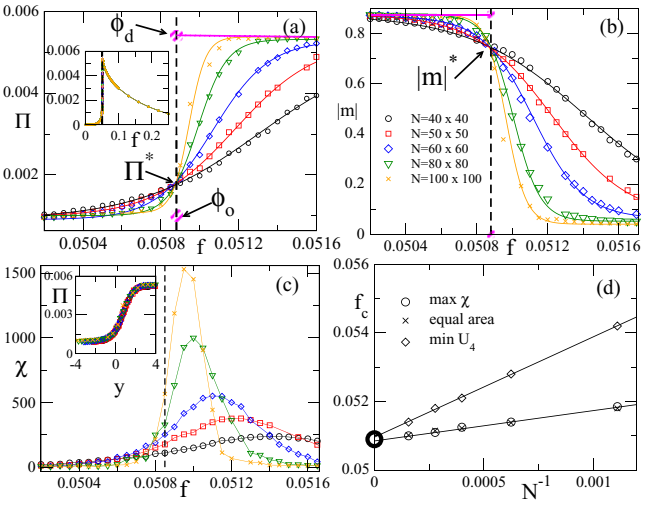

FIG. 5. Bidimensional lattice with $k = 20$ and $\theta = 0.375$. Panels (a–c) show the steady Π, the order parameter $|m|$ and the variance χ versus f, respectively, for distinct system sizes at the vicinity of phase coexistence. Dashed lines: Crossing point among entropy production curves. Continuous lines in (a) and (b) correspond to the theoretical description, Eq. (28). Top and bottom insets: Π for larger sets of f and collapse of data by taking the relation $y = (f - f_0)N$, respectively. In (d), the plot of the maximum of χ, minimum of U_4 and equal area order-parameter probability distribution versus N^{-1}.

Eq. (28) for describing Π at the phase coexistence region. Out of the scaling regime ($f > f_0$ for large N), Π depends solely on the control parameters (f and θ for the MV), as can be seen in the upper inset of Fig. 5. The crossing in both order parameter and entropy production not only discerns the behavior from regular and complex topologies (see, e.g., Fig. 6)

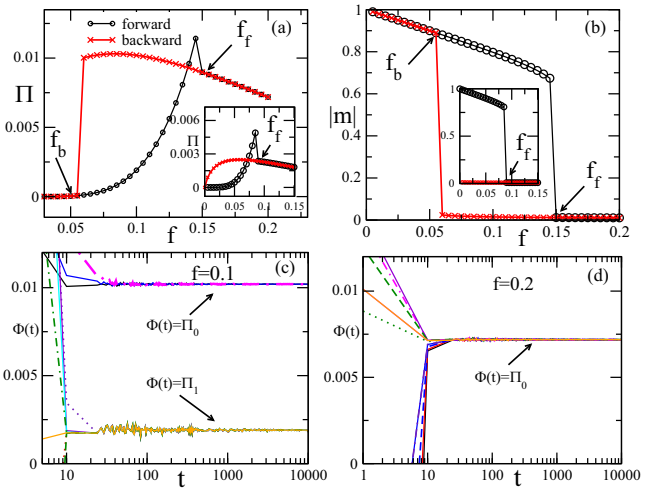

FIG. 6. Panels (a) and (b) show the steady Π and $|m|$ versus f for $k = 20$, $\theta = 0.3$ for the random-regular (RR) case with $N = 10^4$. Black and red curves correspond to the forward and backward "trajectories," respectively. Inset: the same but for $\theta = 0.375$. In panels (c) and (d), the time evolution of $\Phi(t)$ for distinct initial conditions m_0 for $f_b < f = 0.10 < f_f$ and $f = 0.20 > f_f$, respectively. For larger inertia values (inset), the bistability extends over $0 \leqslant f \leqslant f_f$, also viewed from the behavior of steady Π.

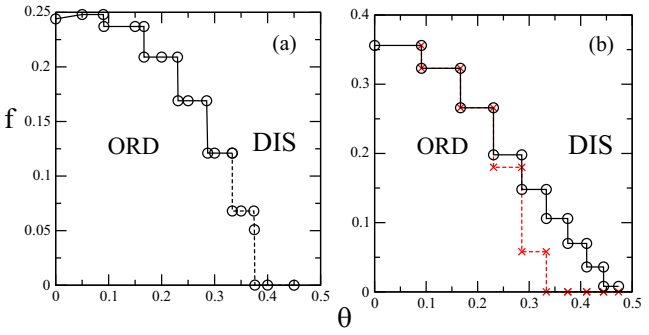

FIG. 7. Panels (a) and (b) show the phase diagrams for $k = 20$ for regular and RR structures, respectively, through analysis of entropy production. ORD (DIS) denote the ordered (disordered) phases and continuous (dashed) lines correspond to continuous (discontinuous) phase transitions. In panel (b), circles ($\times$) correspond to the increase (decrease) of f starting from an ordered (disordered) phase.

but also discontinuous and continuous phase transitions (see, e.g., Fig. 11).

Conversely, Fig. 6 depicts the main results for the MV in a random-regular (RR) topology, for $k = 20, \theta = 0.3$ and $N = 10^4$. In such case, the entropy production reveals typical signatures from aforementioned complex networks: the existence of a hysteretic loop [Fig. 6(a)] located at the interval $f_b = 0.055 < f < f_f = 0.15$, in full equivalence with the order-parameter branch [Fig. 6(b)] [21,23].

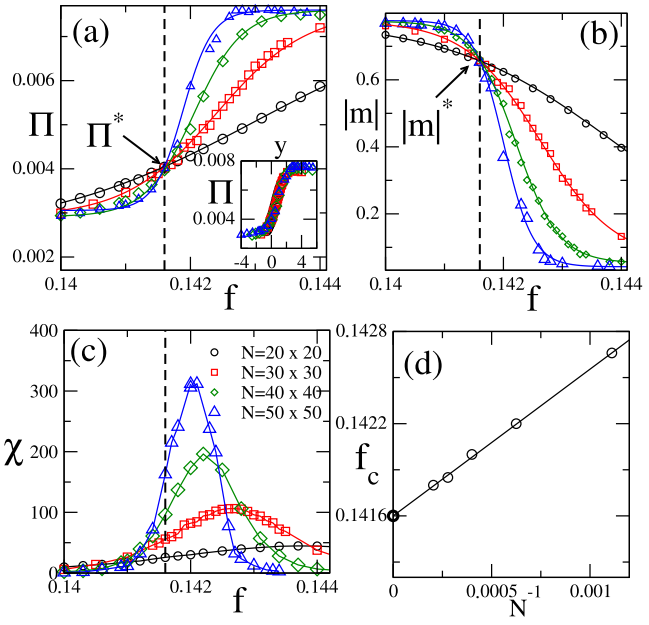

FIG. 8. Regular lattice for $k = 20$ and $\theta = 0.32$: Panels (a)–(c) depict the steady Π, the order parameter $|m|$, and the variance χ versus f, respectively, for distinct system sizes at the vicinity of phase coexistence. Dashed lines: Crossing point among entropy production curves. Continuous lines in (a) and (b) are the theoretical description presented in Eq. (28). Inset: collapse of data by taking the relation $y = (f - f_0)N$. In panel (d), the plot of the maximum of χ versus N^{-1}.

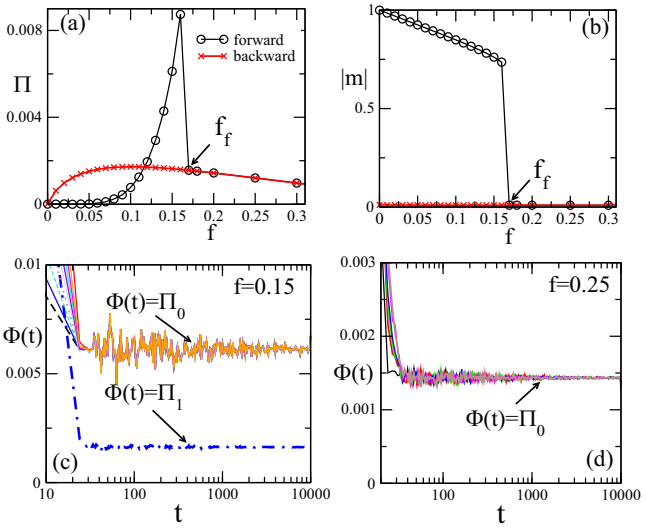

FIG. 9. For the RR structure, panels (a) and (b) show the steady Π and $|m|$ versus f for $k = 20$ and $\theta = 0.35$. In panels (c) and (d), the time evolution of $\Phi(t)$ for distinct initial conditions for $f = 0.15$ (bistable loop) and $f = 0.25$ (disordered phase), respectively.

The phase diagrams, calculated from the entropy production analysis, are shown in Fig. 7 for both regular and complex networks.

Figures 8 and 9 depict the main results for the bidimensional and random-regular structures for $\bar{q} = 3$, in which the C_{3v} symmetry leads to an entirely different critical behavior from the $\bar{q} = 2$ case. However, the phase coexistence portraits are analogous to the previous ones, including the existence of bistability (complex networks), crossing among curves at

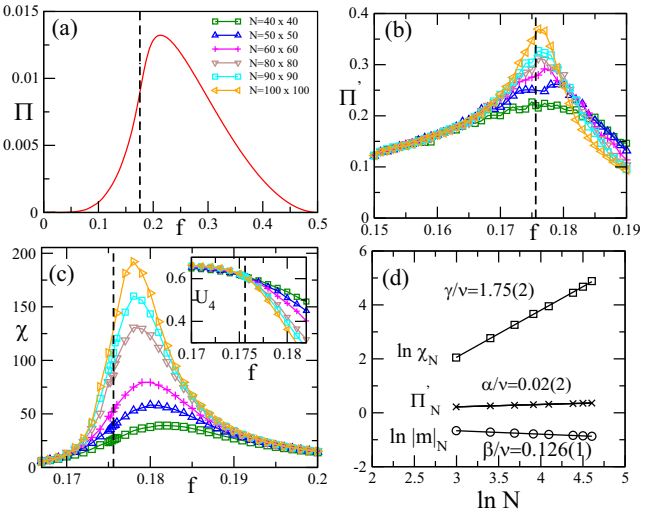

FIG. 10. Regular lattice for interactions between the first to the third next neighbors ($k = 12$) and $\theta = 0.2$: Panels (a)–(c) depict the entropy production Π, its derivative Π' and the variance χ versus f, respectively for distinct system sizes. Inset: the same but for fourth-order reduced cumulant U_4. Dashed lines denote the critical point f_c evaluated through the crossing among U_4 curves. In panel (d), the $\ln \chi_N$, $\ln |m|_N$ and Π'_N versus $\ln N$ at $f = f_c$.

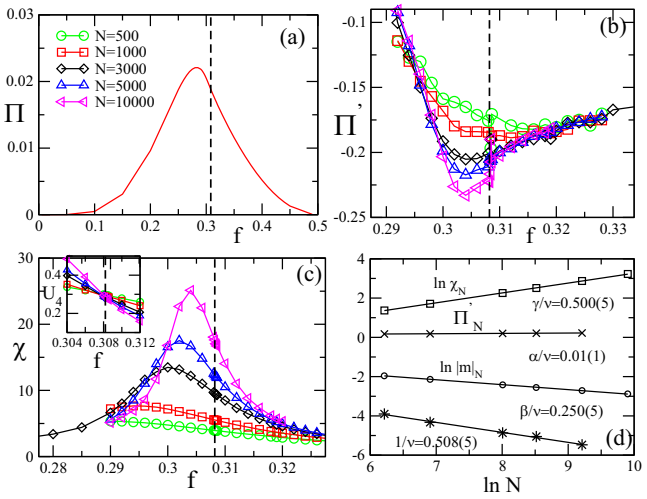

FIG. 11. Random regular (RR) network with $k = 12$ and $\theta = 0$: Panels (a)–(c) show the steady entropy production Π, its derivative Π' and χ versus f for distinct system sizes respectively. Inset: the reduced cumulant U_4 vs. f. Dashed lines denote the critical point f_c evaluated through the crossing among U_4 curves. Panel (d) depicts the plot of $\ln \chi_N$, $\ln |m|_N$, Π'_N and $\ln(f_c - f_N)$ versus $\ln N$ at $f = f_c$.

the transition point [$f_0 = 0.14160(5)$] and scaling with the system volume (regular structures), thereby reinforcing the robustness of our findings at discontinuous phase transitions.

2. *Continuous phase transitions*

Previous results show that irrespectively the value of θ [23], the phase transition remains continuous in regular structures when $k < 20$ whose critical exponents are consistent with the values $\beta = 1/8$, $\gamma = 7/4$, and $1/\nu = 1$ [19]. Figure 10 illustrates continuous phase transition traits in terms of the entropy production. Although Π is finite in the critical point [Fig. 10(a)], Π' increases without limits as $N \to \infty$ [Fig. 10(b)]. For finite systems, Π'_N evaluated at $f = f_c$ increases with $\ln N$, consistent to a logarithmic divergence in which one associates the exponent $\alpha = 0$ [Fig. 10(d)].

Figure 11 extends the analysis for RR structures. In that case, the critical behavior follows the exponents $\beta/\nu = 1/4$, $\gamma/\nu = 1/2$ and $1/\nu = 1/2$ [32], rather different from $\beta = 1/2$, $\gamma = 1$ and $1/\nu = 2$ (MFT) and those from regular lattices (Fig. 10). In similarity to the bidimensional case, $\Pi(f_c)$ is finite and $\Pi'_N(f_c)$ increases with $\ln N$, which is also consistent to a logarithmic divergence and with the exponent $\alpha = 0$. As in Sec. II, such conclusions are reinforced by appealing to the hyperscaling relation $\alpha + 2\beta + \gamma = 2$. Having the values of β and γ, we reobtain in both cases $\alpha = 0$. Last, the $\bar{q} = 3$ case is characterized in regular lattices by the critical exponents $\beta = 1/9$ and $\gamma = 13/9$. According to the hyperscaling relation, the exponent associated with the entropy production should read $\alpha = 1/3$. Very recently, the value $\alpha = 0.32(2)$ has been confirmed from numerical simulations in Ref. [33], in full accordance with our theoretical predictions. The present analysis not only puts on firmer basis the behavior of entropy production at the criticality but also extends the hyperscaling relation for nonequilibrium phase transitions.

V. CONCLUSIONS

Based on general considerations, the description of entropy production at continuous and discontinuous (practically unexplored) phase transitions was presented. Our main findings are that continuous and discontinuous phase transitions can be classified through specific (well defined) entropy production traits in the realm of MFT and beyond MFT. Our approach embraces fundamental aspects comprising the influence of the lattice topology and symmetry properties. At the phase coexistence, the entropy production presents a discontinuity in a single (and well defined) point in regular lattices, whereas a hysteretic loop is portrayed in complex networks. The former case is also characterized by the existence of a crossing point among entropy production curves for distinct system sizes. A general description of entropy production in the framework of mean-field theory for systems with Z_2 symmetry was presented. Our work is a relevant step in trying to unify the description of nonequilibrium phase transitions through a key indicator of system irreversibility. As a final comment, it would be interesting to consider the critical behavior of entropy production (and its allied quantities) for systems displaying other symmetries and universality classes, to verify the reliability of finite size ideas presented here.

ACKNOWLEDGMENT

C.E.F. and P.E.H. acknowledge the financial support from FAPESP under Grants No. 2018/02405-1 and No. 2017/24567-0, respectively.

[1] I. Prigogine, *Introduction to Thermodynamics of Irreversible Processes*, 2nd ed. (Wiley, New York, 1961).
[2] S. R. de Groot and P. Mazur, *Non-Equilibrium Thermodynamics* (North-Holland, Amsterdam, 1962).
[3] U. Seifert, Rep. Prog. Phys. **75**, 126001 (2012).
[4] L. Crochik and T. Tomé, Phys. Rev. E **72**, 057103 (2005).
[5] T. Tomé and M. J. de Oliveira, Phys. Rev. Lett. **108**, 020601 (2012).
[6] T. Tomé and M. J. de Oliveira, Phys. Rev. E. **91**, 042140 (2015).
[7] Y. Zhang and A. C. Barato, J. Stat. Mech. (2016) 113207.
[8] B. Andrae, J. Cremer, T. Reichenbach, and E. Frey, Phys. Rev. Lett. **104**, 218102 (2010).
[9] D. Mandal, K. Klymko, and M. R. DeWeese, Phys. Rev. Lett **119**, 258001 (2017).
[10] M. Brunelli, L. Fusco, W. Wieczorek, J. Hoelscher-Obermaier, G. Landi, F. L. Semiao, A. Ferraro, N. Kiesel, T. Donner, G. De Chiara, and M. Paternostro, Phys. Rev. Lett **121**, 160604 (2018).
[11] J. Schnakenberg, Rev. Mod. Phys. **48**, 571 (1976).
[12] P. Gaspard, J. Chem. Phys. **120**, 8898 (2004).
[13] H. Ge and H. Qian, J. R. Soc. Int. **8**, 107 (2011).

[14] A. Imparato, New J. Phys. **17**, 125004 (2015).
[15] P. S. Shim, H. M. Chun, and J. D. Noh, Phys. Rev E **93**, 012113 (2016).
[16] T. Herpich, J. Thingna, and M. Esposito, Phys. Rev. X **8**, 031056 (2018).
[17] T. Herpich and M. Esposito, Phys. Rev. E **99**, 022135 (2019).
[18] A. C. Barato and H. Hinrichsen, J. Phys. A **45**, 115005 (2012).
[19] M. J. de Oliveira, J. Stat. Phys. **66**, 273 (1992).
[20] H. Chen, C. Shen, G. He, H. Zhang and Z. Hou, Phys Rev. E **91**, 022816 (2015).
[21] H. Chen, C. Shen, H. Zhang, G. Li, Z. Hou, and J. Kurths, Phys Rev. E **95**, 042304 (2017).
[22] P. E. Harunari, M. M. de Oliveira, and C. E. Fiore, Phys Rev. E **96**, 042305 (2017).
[23] J. M. Encinas, P. E. Harunari, M. M. de Oliveira, and C. E. Fiore, Sci. Rep. **8**, 9338 (2018).
[24] T. Tomé and M. J. de Oliveira, *Stochastic Dynamics and Irreversibility* (Springer, Cham, 2015).
[25] M. M. de Oliveira, M. G. E. da Luz, and C. E. Fiore, Phys. Rev. E **97**, 060101(R) (2018).
[26] M. M. de Oliveira, M. G. E. da Luz, and C. E. Fiore, Phys. Rev. E **92**, 062126 (2015).
[27] M. S. S. Challa, D. P. Landau, and K. Binder, Phys. Rev. B **34**, 1841 (1986).
[28] M. Pineda and M. Stamatakis, Entropy **20**, 811 (2018).
[29] See e.g. J. Gómez-Gardeñes, S. Gómez, A. Arenas, and Y. Moreno, Phys. Rev. Lett. **106**, 128701 (2011).
[30] A. Fronczak and P. Fronczak, Phys. Rev. E **96**, 012304 (2017).
[31] B. Bollobás, Eur. J. Combinator. **1**, 311 (1980).
[32] L. F. C. Pereira and F. G. Brady Moreira, Phys. Rev. E **71**, 016123 (2005).
[33] O. A. Barbosa Bohórquez *et al.*, J. Phys. A: Math. Theor. (2019), doi: 10.1088/1751-8121/ab2640.